energies

Article

Dynamic Simulation Model of a Prosumer Building with PV, CHP, Thermal Storage and Electric Vehicle Charging Points

Stefano Bracco *, Matteo Fresia, Tommaso Robbiano, Federico Silvestro and Stefano Massucco

Department of Electrical, Electronics and Telecommunication Engineering and Naval Architecture (DITEN), University of Genoa, Italy, Via Opera Pia 11a, 16145 Genoa, Italy; matteo.fresia@edu.unige.it (M.F.); tommaso.robbiano@edu.unige.it (T.R.); federico.silvestro@unige.it (F.S.); stefano.massucco@unige.it (S.M.)

* Correspondence: stefano.bracco@unige.it; Tel.: +39-01921945123

Abstract

One of the ways to decarbonize cities and to enhance grid stability is to convert existing buildings into prosumers equipped with power plants able to supply electrical and thermal energy. The simulation of such multi-energy systems permits the analysis of their performance in steady-state and dynamic conditions, with the aim of defining effective operating strategies able to reduce emissions and costs. The present paper describes a dynamic simulation model, implemented in the Matlab/Simulink R2025a environment, developed to simulate the daily and weekly operation of a prosumer building equipped with a small-sized cogeneration unit, a Photovoltaic (PV) plant, a back-up boiler, a thermal storage system and some charging points for Electric Vehicles (EVs). The mathematical model is reported in detail, and the main results of the study are described, referring to operating days characterized by different weather conditions. Then, energy, economic and environmental performance indicators are defined and calculated for the different simulated scenarios. Over the considered time horizons, the simulation results highlight a significant increase in the electrical self-sufficiency of the facility up to 91.1% and an important reduction in total net operating costs up to 59.8%, compared to the *AS-IS* case (i.e., without the newly installed technologies).

Keywords: simulation; prosumer; microturbine; cogeneration; photovoltaics; storage; electric vehicles

1. Introduction

The global transition toward sustainable energy systems has prompted significant shifts in how buildings interact with utility grids. Modern buildings are increasingly evolving from passive energy consumers to active prosumers, entities that both produce and consume energy through Distributed Generation (DG) technologies. This transformation is pivotal in alleviating loads on national electricity networks while enhancing overall energy security and reducing carbon emissions. Prosumer buildings equipped with Renewable Energy Sources (RESs), Combined Heat and Power (CHP) systems, and various storage technologies represent a promising pathway toward decentralized, efficient, and environmentally sustainable energy systems [1].

Among various DG sources, Photovoltaic (PV) systems are particularly well-suited for integration into residential and commercial buildings. Meanwhile, CHP systems, especially Microturbines (MTs), offer high energy efficiency by simultaneously generating electrical and thermal energy to meet the demands of buildings. To further enhance the

Check for updates

Received: 31 December 2025
Revised: 11 February 2026
Accepted: 13 February 2026
Published: 19 February 2026

self-consumption of locally generated renewable energy and improve energy management, the integration of thermal storage and Electric Vehicle (EV) charging infrastructures in prosumer buildings has attracted significant attention. Thermal storage can store excess thermal energy produced by CHP systems or captured by solar thermal collectors for later use. At the same time, EV charging points enable prosumers to utilize their on-site electricity generation for transportation needs.

The combined operation of these technologies presents significant challenges in terms of system sizing, control strategies, and energy management approaches. CHP systems must balance electrical and thermal outputs to meet building demands efficiently, with operating strategies critically affecting performance metrics including primary energy consumption, CO_2 emissions, and operational costs [2,3]. Meanwhile, the intermittent nature of PV generation necessitates intelligent integration with storage systems and/or grid exchange mechanisms to maximize self-consumption and economic benefits [4].

Integrating RESs like solar and wind with CHP systems further reduces reliance on fossil fuels and mitigates environmental impact, improving energy efficiency and reducing emissions. MTs are a key component of CHP systems, offering the ability to burn various fuels at high and low-pressure levels. While they may have slightly lower electrical efficiencies than reciprocating engine generators, their design simplicity, higher reliability, reduced noise and vibration, lower maintenance requirements, and lower emissions make them an attractive option [5]. CHP units are critical coupling components in multi-energy systems, and modelling and simulation studies of the CHP operation are fundamental for energy and economic analyses. The authors in [6] developed a dynamic model of a University Campus micro-CHP plant in Thermolib and Simulink environments. They modelled a methane gas engine based on the Otto cycle and validated the electrical and thermal outputs against real operational data, noting discrepancies in the auxiliary boiler model that required further control system refinement. Study [7] focuses on micro-CHP systems, specifically modelling a CAPSTONE C30 micro gas turbine coupled with a compact heat exchanger and absorption chiller. The thermodynamic analytic model, validated experimentally, effectively predicted performance at partial-load conditions, facilitating the design of trigeneration systems. The paper [8] investigates a flexible district heating network comprising a CHP plant, a peak load boiler and a thermal storage by implementing a Matlab simulation model. A techno-economic comparison between a wood gas and a natural gas CHP plant is presented, giving information about the operating behaviour of various components, in order to suggest potential improvements in terms of efficiency and flexibility for biomass district heating. In [9], a quasi-steady-state simulation model of a biomass CHP plant connected to a district heating network in Liège, Belgium, is presented. The authors evaluate the “cost of heat” to determine economic viability, comparing the CHP plant against standard natural gas boilers. The developed model includes detailed combustion calculations and accounts for heat transport losses in the network. The authors in [10] explore small-scale trigeneration systems by developing a techno-economic optimization method of a Combined Cooling, Heating and Power (CCHP) plant based on an internal combustion engine or a gas turbine as a power system and with an absorption or vapour-compression refrigeration unit. By using the object-oriented Modelica programming language, a program solution was implemented to simulate dynamic behaviours and optimize for energy efficiency, economic payback, and greenhouse gas reductions. To achieve operating optimization for a CHP system featuring a high back-pressure unit and an extraction heating unit, the paper [11] proposes an advanced optimization method using artificial neural networks and simulation databases. To manage the computational load of optimizing the considered system, an integrated approach was implemented through a chaos particle swarm optimization algorithm to generate optimal data points, which in turn are used to train the artificial neural network, and improve the flexibility of CHP systems by predicting their partial-load performance.

The study [12] discusses the optimization of stand-alone hybrid CHP systems, highlighting the impact of power management strategies on system sizing and operation. They compare systems sized using single- vs. multi-objective genetic algorithm optimization, minimizing cost and maximizing efficiency. The authors in [13] address optimizing CHP systems in microgrids based on renewable energy, using wind turbines and PV modules. The study demonstrates that using renewable sources and proper planning of CHP and battery systems with energy management systems significantly reduces microgrid costs and environmental pollution.

In [14], a case study on transforming a residential building cluster in Sweden into electricity prosumers, using PV, centralized variable-speed heat pumps, and DC microgrids with thermal energy storage, is presented. The study demonstrates the feasibility of converting existing buildings into smart electricity prosumers with higher self-consumption rates and energy efficiency.

Energy storage systems play a fundamental role in enabling the reliable and economic integration of intermittent RESs. The study [15] analyses optimizing energy storage capacity in autonomous microgrids, considering CHP and EV scheduling, with the aim to develop strategies for sizing energy sources and storage devices to meet load demands reliably while reducing costs and environmental impact. Optimizing energy management in smart cities has always been challenging for utilities and consumers. However, it can be effectively addressed by optimally sizing and allocating RESs in distribution networks, also with the help of demand-side management, to minimize electricity bills and power losses while taking into account reduction in carbon emissions and peak-to-average ratio of the load [16,17]. In [18], a model for the optimal capacity planning and operation of grid-connected hybrid energy systems with EV charging stations is presented, considering Demand Response (DR) and net energy metering strategies for a case study of a multi-residential complex building with electrical and thermal loads. The optimization objectives minimize system costs and utility bills, and the findings demonstrate that implementing DR programs and making full use of the building roof's maximum PV capacity reduce the amount of electricity withdrawn from the external grid and increase the use of the on-site CHP generator and batteries.

Efficient energy management and control systems are essential for the effective operation of microgrids. Ref. [19] propose energy management models for microgrids with CHP and PV prosumers, using game-theory approaches to optimize pricing and improve load characteristics.

The paper [20] analyses the potential of combined solar-cogeneration installations for residential buildings, finding that integrating thermal solar collectors and micro-gas turbines can maximize energy, economic, and environmental savings, with payback periods under 8 years. In [21], a daily simulation model for analysing natural gas MT applications in residential complexes is presented, considering electrical and thermal efficiency and consumer load curves. The model supports investment decisions by simulating various scenarios. The authors in [22] explored the optimization of micro-gas turbines for CHP applications in low-energy buildings. The results indicate that increasing the turbine inlet temperature improves exergy efficiency and net power output, but also increases costs beyond certain limits due to material constraints. This highlights the role of optimized CHP systems as a stable alternative or additional technology to solar-based nearly zero-energy building designs, particularly where thermal demand is significant.

The paper [23] describes a detailed model of an MT plant that can assess the impact of DG penetration in distribution networks. It shows that replacing simplified MT models with detailed ones allows for more realistic simulations of DG behaviour during grid disturbances. In [24], an economic sensitivity analysis is performed to examine how MTs and PV systems affect total generation costs.

A primary focus of recent research is the direct coupling of building-integrated PV with EV charging infrastructure. The authors in [25] analyzed a building-integrated PV system for a residential building, comparing grid-connected systems with and without battery storage. The paper [26] extended this concept by studying building-integrated PV/thermal collectors in a hotel in Italy. This system produces both electricity and thermal energy for space heating and hot water. The results show that, coupled with an EV charging point, it can significantly reduce primary energy consumption and CO_2 emissions compared to a reference system where the electrical load of the building is completely met by the external grid and a diesel vehicle is considered.

In [27], the authors deeply investigated a prosumer building with a micro-CHP system, PV technology and an electrical storage system with the aim of identifying the prosumer configurations having the highest values of self-coverage of the energy demand, while in [28], a hybrid renewable energy system equipped with a Stirling engine micro-CHP unit fed by biomass and PV-thermal collectors was analysed by considering its possible installation under different climate and economic conditions. The optimal integration of a micro-CHP system with an electrical storage system is also investigated in [29], whereas in [30] the focus is on the integration of hydrogen technologies with PV plants in buildings.

The modelling of multi-energy systems requires robust frameworks to handle the heterogeneity of different energy vectors and their interactions across various time scales. The authors in [31] introduce an open-source multi-energy system simulator, comparing it to a benchmark optimization model, to investigate the advantages and disadvantages of simulating energy systems with respect to an optimization approach. The outcomes demonstrate that a simulation approach can be used to analyse multi-energy systems at an urban level with satisfactory results. In [32], a new multi-energy coupling interface modelling method is proposed to handle the strong coupling between electrical, mechanical and thermal subsystems, applying it to a 300 MW cogeneration reheating motor set. Paper [33] proposes a simulation-based methodology to assess flexibility in multi-energy systems, specifically within district heating networks, characterised by a thermal demand, a distribution thermal network and a central power plant composed of a cogeneration unit and a gas boiler. The authors distinguish between physical flexibility (system limits) and operational flexibility (modulation capability), demonstrating how network dynamics constrain the flexibility available to the grid. In [34], the authors model PV prosumers integrated with stationary batteries, heat pumps and EVs across 145 global regions. They found that by 2050, such prosumer systems could provide the least-cost energy solution in many regions, with batteries and thermal storage playing key roles in optimizing self-consumption. An economic model predictive control strategy for an office building integrated with PV, heat pumps, thermal tanks and electric buses is investigated in [35], using a resistance-capacitance model for building thermal dynamics. The proposed strategy outperformed traditional rule-based control, reducing daily costs up to 26.95% and significantly improving peak load reduction by leveraging the mobile storage capability of electric buses.

The present study has been developed with the aim of proposing a dynamic simulation model of a prosumer building characterized by the presence of a PV plant, a CHP unit, a thermal storage system, a back-up boiler and some charging points for EVs. The paper reports all the equations used to model the aforesaid subsystems and provides information on their implementation in the Matlab/Simulink R2025a environment.

The developed model is not an optimization-based Energy Management System, but it represents a dynamic simulation model based on some heuristic rules regarding the

https://doi.org/10.3390/en19041064

operation of the installed technologies. In particular, the CHP unit, based on MT technology, is operated in "electrical priority" mode, while the boiler is turned on when the CHP unit and the thermal storage system cannot cover the whole heating demand of the building. The EVs are not charged by implementing smart charging strategies since, once they arrive at the facility, they are immediately charged.

The different components of the considered multi-energy system are modelled using not only algebraic equations but also differential equations that permit the representation of dynamic phenomena, such as accumulation of mass, kinetic energy, and thermal energy. Moreover, suitable control systems based on PID controllers have been implemented to optimize the operation of power plants and to maintain a desired comfort inside the building. The proposed model is generally valid and, due to its interconnected subsystem structure, can be applied to other prosumer configurations. It can also accommodate new subsystems representing technologies that were not considered in this study.

A strong scientific contribution of the present paper is analysing the interaction and behaviour of different technologies in a multi-energy system to satisfy thermal and electrical demands of the case study building, by developing a detailed dynamic modelling of most of the components to take into account thermal and electrical dynamics. To the authors' knowledge, no other similar studies proposed a mathematical simulation model covering a complex multi-energy system such as the one considered, including PV plants, CHP units, thermal storage, back-up boiler and EV charging points, and technically describing in detail the coupling of electrical and thermal subsystems with the corresponding controllers to adjust and optimize their operation to meet the prosumer building's requests in terms of comfort (i.e., temperature inside the building), electrical and thermal energy needs. In particular, the validation of the CHP model, including the dual-PID control strategy and the corresponding parameter tuning, has been done through experimental tests carried out on the two CAPSTONE C65 microturbines installed at the Savona Campus microgrid of the University of Genoa (Italy). Results of the validation phase can be found in the paper [36] which represents the starting point of the research developed in this scientific area.

To provide a comprehensive overview of the study's scope and to refine future investigative frameworks, certain limitations of the developed work should be acknowledged and identified. Concerning the operating mode of the CHP unit, only the "electrical priority mode" is considered, since the inclusion of the thermal storage and the back-up boiler already offers a slack source in case the CHP unit is not able to provide the needed thermal power. Still, the authors intend to improve the simulation model, taking into account also the influence of adopting a "thermal priority mode" in future studies. To reduce the computational effort without compromising the validity of the results, as also proved by the validation phase of the CHP model reported in [36], a unique mass accumulation block has been modelled to represent the mass accumulation in all the MT components; moreover, the turbine has been considered always operated in chocking mode. Regarding the EVs' charging, EVs start immediately charging once they are connected to the available charging points, and no smart charging and vehicle-to-grid/vehicle-to-building strategies have been implemented in the present work.

The remainder of the paper is as follows. Section 2 describes the methodology by presenting the mathematical model alongside the various hypotheses and assumptions employed to represent the different subsystems. Section 3 is devoted to discussing the results by analysing how the prosumer operates in different daily and weekly scenarios and by evaluating its performance through calculating some energy, economic and environmental indicators. Finally, Section 4 reports the main conclusions of the study.

2. Materials and Methods

The main goal of the research was to develop a dynamic simulation mathematical model capable of representing the behaviour over time of a complex energy system consisting of a prosumer building whose electrical and thermal needs are met by a hybrid energy system characterized by a PV plant, an MT acting as a CHP unit, a thermal storage system, and a boiler. In addition, the building is connected to the distribution network and can draw electricity from it or feed electricity into it, depending on the difference between the electricity produced locally and that required by the loads. The loads include not only the electrical appliances installed in the building, but also some charging points for EVs owned by the building's occupants. The mathematical model, described by differential and algebraic equations, has been implemented in the Matlab/Simulink R2025a environment [37] by organising it into the set of the subsystems reported in the information diagram shown in Figure 1 and here below listed:

- Load: this block represents the electrical load profile of the building which can be defined by the user through the analysis of historical data, possibly corrected with information on weather and occupancy level of the building.
- PV: it is the subsystem used to calculate the power production of the PV plant as a function of the solar irradiance profile and technical data of the installed plant (number of modules installed on the roof, azimuth and tilt angles, etc.).
- EV: this subsystem generates the charging power profiles required by the EVs present at the facility as a function of both their state of charge at the arrival and the technical data of each vehicle (rated capacity of the battery, maximum charging power, etc.).
- EL_B: through this block, which acts as a sort of electrical energy balance for the whole system, it is possible to calculate at any time the power withdrawn from/injected into the public distribution network and the electrical power reference profile for the MT which is operated in "electrical priority" mode.
- CHP: within this block there are several nested subsystems, one for each component of the MT (compressor, recuperator, combustion chamber, turbine, shaft, heat recovery boiler, etc.), which are used to calculate all the main physical quantities (mainly pressure, temperature and flow rate) that describe the operation of the MT.
- CHP_CS: it is the subsystem where the control system of the MT is implemented. Its function is to regulate the fuel flow rate in order to follow the electrical power reference profile provided by the EL_B block.
- PB: this subsystem models the thermal dynamic behaviour of the building in order to evaluate how the indoor temperature changes as a function of time.
- PB_CS: it represents the thermal control system of the building, the aim of which is to estimate the thermal flux required to maintain a certain desired temperature inside the building.
- STO: this system is used to model the dynamics of the thermal storage system which is installed to balance the local thermal production of the MT and the thermal power requested by the building. The storage system can be either charged or discharged.
- Boiler: a back-up boiler is installed to provide thermal energy when both the MT and the storage are unable to fully meet the thermal needs of the building. It acts as a sort of thermal slack.

  The main equations used to model the above subsystems are presented and described below.

https://doi.org/10.3390/en19041064

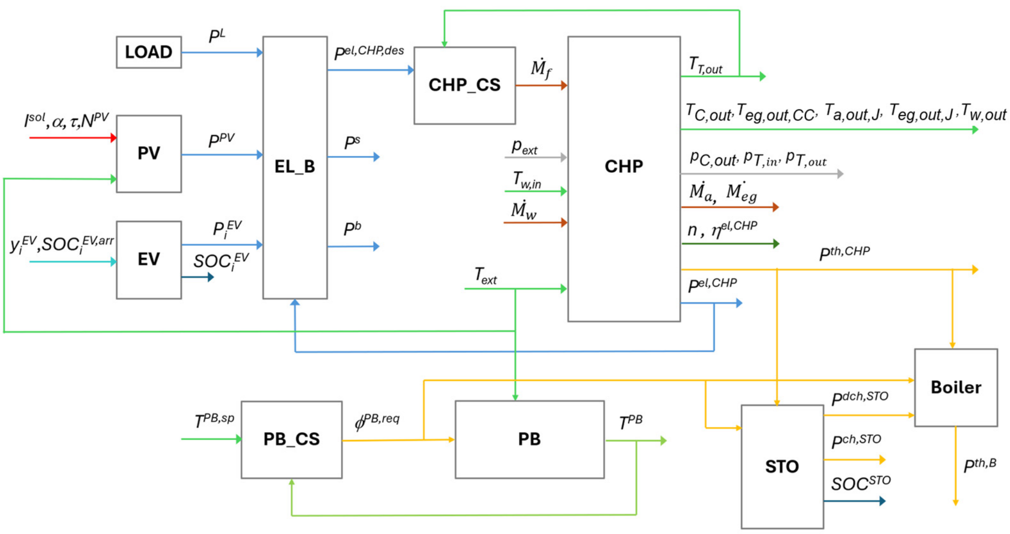

Figure 1. Information diagram of the dynamic simulation model.

2.1. Load

The electrical load is represented by all the devices which consume electricity inside the building. In particular, we refer to the interior and exterior lighting system and a variety of electrical appliances (computers, printers, washing machines, ovens, dishwashers, refrigerators, small household appliances, etc.). The user can provide the electrical load profile in a form of a vector of power demand values accompanied by the corresponding times. The total electrical load of the building is indicated by P^L.

2.2. PV Plant

The electrical power P^{PV} generated by the PV plant installed on the roof of the building is calculated as a function of the solar irradiance profile I^{sol}, the azimuth (α) and tilt (τ) angles which describe the installation of the modules on the roof, the number of modules N^{PV} and the external ambient temperature T_{ext} [38]:

$$P^{PV} = P^{PV}\left(I^{sol}, \alpha, \tau, N^{PV}, T_{ext}\right) \tag{1}$$

2.3. EV Charging

I different EVs can be charged at the facility, each one using a dedicated AC charging point. The main data describing the i-th vehicle are represented by the rated capacity of the battery (C_i^{EV}), the rated charging power ($P_i^{EV,max}$) and the indicator y_i^{EV} which is equal to 1 if the EV is present at the facility and can therefore be charged, and is zero otherwise. The model assumes that the charging power P_i^{EV}, the quantities on which it depends being given in (2), is lower than the rated one when the State Of Charge (SOC_i^{EV}) is higher than a limit value identified by $SOC_i^{EV,lim}$, thus modelling the real charging behaviour.

$$P_i^{EV} = P_i^{EV}\left(y_i^{EV}, SOC_i^{EV,arr}, SOC_i^{EV}, SOC_i^{EV,lim}, C_i^{EV}, P_i^{EV,max}\right) \tag{2}$$

SOC_i^{EV} is obtained by integrating the differential equation given in (3), which represents the energy balance of the battery. To solve it, both the SOC_i^{EV} at the arrival time ($SOC_i^{EV,arr}$) and the charging efficiency $\eta^{ch,EV}$ must be known.

$$\frac{dSOC_i^{EV}}{dt} = \frac{\eta^{ch,EV} \cdot P_i^{EV}}{C_i^{EV}} \tag{3}$$

2.4. Electrical Balance

The main inputs of this subsystem are: the building's electrical load P^L, the PV power production P^{PV}, the charging power supplied to each EV (P_i^{EV}) and the electrical power generated by the MT ($P^{el,CHP}$), this last calculated by the CHP subsystem. Depending on whether local generation is less or more than the total load, (4) and (5) are activated to calculate the power absorbed by (P^b) or injected into (P^s) the public distribution network to which the prosumer building is connected.

$$P^b = max\left(0\ ;\ P^L + \sum_{i=1}^{I} P_i^{EV} - P^{PV} - P^{el,CHP}\right) \tag{4}$$

$$P^s = max\left(0\ ; -P^L - \sum_{i=1}^{I} P_i^{EV} + P^{PV} + P^{el,CHP}\right) \tag{5}$$

On the other hand, the reference electrical power for the MT control system is calculated according to (6), where $P^{el,CHP,max}$ is the maximum electrical power that the MT can produce at the current ambient temperature, while $P^{el,CHP,min}$ is the minimum electrical power (usually referred to as the "technical minimum") below which the manufacturer suggests to switch off the MT. From analysing (4) and (6), it appears that it is preferable to use the MT instead of buying electricity from the public network, whenever it is possible.

$$P^{el,CHP,des} = max\left(P^{el,CHP,min}\ ;\ min\left(P^{el,CHP,max}\ ;\ P^L + \sum_{i=1}^{I} P_i^{EV} - P^{PV}\right)\right) \tag{6}$$

2.5. CHP Plant

The present simulation model assumes that the MT works in "electrical priority" mode, since the main aim of the prosumer building is that of limiting the purchase of electricity from the public distribution network. Consequently, if the thermal power produced by the MT is not sufficient to fully meet the building thermal energy needs, additional energy comes from either the thermal storage, operating in discharging mode, or the boiler. If the building requires less thermal energy than is produced, the excess is stored or dissipated, simulating the opening of the flue gas bypass typically fitted to modern MTs, to avoid the passing of exhaust gases through the hot water heat exchanger. The validation of the CHP model has been done using real data collected at the Savona Campus microgrid of the University of Genoa (Italy) and discussed as reported in a previous research study [36]. The main equations used to model the different parts of the MT are deeply investigated in the following.

2.5.1. Compressor

Following the approach adopted by the authors in [36], the compressor (C) has been modelled as an algebraic block through its two characteristic maps that plot, respectively, the pressure ratio $\left(\frac{p_{C,out}}{p_{C,in}}\right)$ as a function of the reduced speed $\left(\frac{n}{\sqrt{T_{C,in}}}\right)$ and the reduced mass flow rate $\left(\frac{\dot{M}_{a,C}\cdot\sqrt{T_{C,in}}}{p_{C,in}}\right)$, and the adiabatic efficiency (η_C) as a function of the reduced speed and the pressure ratio. As indicated in (7), the first map receives in input the pressure ratio, the reduced speed and the temperature and pressure at the inlet of the compressor to obtain the air mass flow rate ($\dot{M}_{a,C}$), while the second map is used to evaulate the efficiency on the basis of the reduced speed and the pressure ratio, as shown in (8).

$$\dot{M}_{a,C} = \dot{M}_{a,C}(p_{C,in}, p_{C,out}, n, T_{C,in}) \tag{7}$$

$$\eta_C = \eta_C(p_{C,in}, p_{C,out}, n, T_{C,in}) \tag{8}$$

The temperature at the outlet of the compressor ($T_{C,out}$) is calculated as follows:

$$T_{C,out} = T_{C,in} \cdot \left[1 + \frac{\left(\frac{p_{C,out}}{p_{C,in}}\right)^{\frac{k_C - 1}{k_C}} - 1}{\eta_C} \right] \tag{9}$$

where k_C is the adiabatic exponent, which is given by the ratio between the average specific heat at constant pressure and that at constant volume of the air flowing through the compressor. The real power absorbed by the compressor is computed as:

$$P_C = \dot{M}_{a,C} \cdot \bar{c}_{p,a,C} \cdot (T_{C,out} - T_{C,in}) \tag{10}$$

where $\bar{c}_{p,a,C}$ is air average specific heat at constant pressure.

In order to represent the dynamic phenomena of mass and kinetic energy accumulation occurring in the MT under transient operating conditions, it was decided to insert the two dummy components shown in Figure 2 between the compressor and the recuperator and to adopt an electrical-mechanical analogy approach to model them [36]. The first, denoted by Ψ_f, represents the accumulation of mass within the whole MT, where Ψ_f is a fluid-dynamic capacitance (equal to the ratio between the overall accumulation volume and the squared speed of sound within the considered fluid), while the second, denoted by Λ_f, emulates the accumulation of kinetic energy within the whole MT, where Λ_f is a fluid-dynamic inductance (evaluated as the ratio between an equivalent length, representing the fluid path within the MT, and an average cross section).

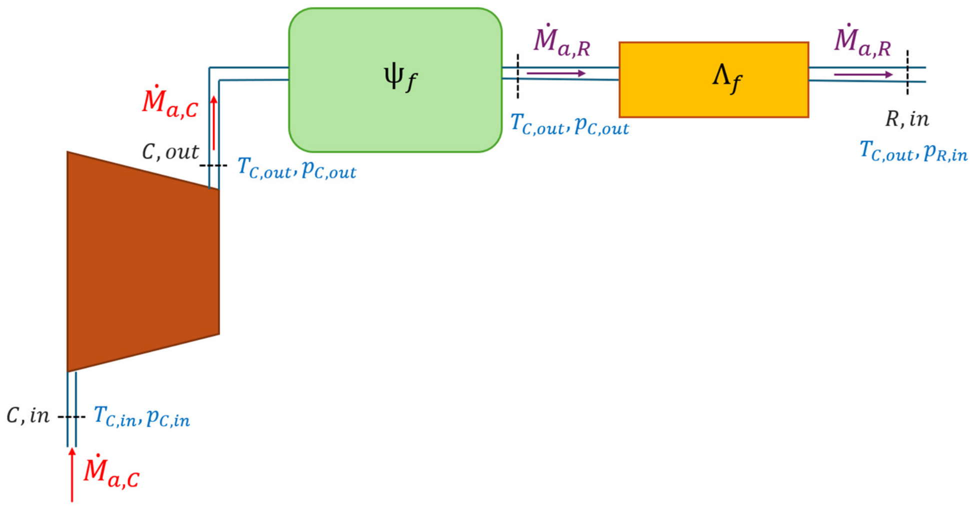

Figure 2. Scheme used to study the compressor and the associated dynamic blocks.

The fluid-dynamic capacitance block appears in the differential Equation (11) which, when properly integrated, gives the pressure at the outlet of the compressor ($p_{C,out}$), since no pressure drop is taken into account inside the mass accumulation block.

$$\frac{dp_{C,out}}{dt} = \frac{1}{\psi_f} \cdot \left(\dot{M}_{a,C} - \dot{M}_{a,R} \right) \tag{11}$$

The air mass flow rate ($\dot{M}_{a,R}$) through the recuperator is obtained by integrating the differential equation used to model the inductance block:

$$\frac{d\dot{M}_{a,R}}{dt} = \frac{1}{\Lambda_f} \cdot (p_{C,out} - p_{R,in}) \tag{12}$$

where the air pressure ($p_{R,in}$) at the inlet of the recuperator is higher than the pressure ($p_{T,in}$) of the exhaust gas at the inlet of the turbine, in order to correctly taking into account, albeit in a simple way, the pressure drop occurring in the recuperator and the combustion chamber:

$$p_{R,in} = p_{T,in} \cdot \left(1 + \gamma \cdot \dot{M}_{a,R}^2\right) \tag{13}$$

γ being a proportionality coefficient related to the operation of the MT at steady-state full load.

2.5.2. Recuperator

As is well know, the recuperator (R) can be studied as a gas-gas counterflow heat exchanger that enables the transfer of heat from exhaust gas exiting the turbine to the air coming from the compressor. In order to properly model the thermal energy accumulation in the metal part of the recuperator during transient conditions, the heat exchanger has been divided lengthwise into J parts, each characterised by a different temperature ($T_{m,j}$) at each time. The temperature $T_{m,j}$ is calculated by integrating the following differential equation:

$$\frac{dT_{m,j}}{dt} = \frac{1}{C_{m,j}} \cdot (\phi_{eg,m,j} - \phi_{m,a,j}) \tag{14}$$

where $C_{m,j}$ is the metal heat capacity (given by the multiplication between the mass of the j-th metal part and its specific heat), while $\phi_{eg,m,j}$ and $\phi_{m,a,j}$ are the heat flux given to the metal by the exhaust gas and that given off by the metal to the air, respectively, calculated according to (15) and (16).

$$\phi_{eg,m,j} = \dot{M}_{eg} \cdot \overline{c}_{p,eg,j} \cdot (T_{eg,in,j} - T_{eg,out,j}) = K_{eg,m} \cdot S_{eg,m} \cdot \Delta T_{lm,eg,m} \tag{15}$$

$$\phi_{m,a,j} = \dot{M}_{a,R} \cdot \overline{c}_{p,a,j} \cdot (T_{a,out,j} - T_{a,in,j}) = K_{a,m} \cdot S_{a,m} \cdot \Delta T_{lm,a,m} \tag{16}$$

In (15) $\dot{M}_{eg}$ is the exhaust gas mass flow rate, $\overline{c}_{p,eg,j}$ is the average specific heat at constant pressure of the exhaust gas, while $T_{eg,in,j}$ and $T_{eg,out,j}$ indicate the exhaust gas temperature at the inlet/outlet of the j-th part of the recuperator, respectively. Similar considerations can be drawn for the heat flux provided by the metal to the air, as described in (16), where $\overline{c}_{p,a,j}$ is the average specific heat at constant pressure of air, $T_{a,in,j}$ and $T_{a,out,j}$ represent the air temperature at the inlet/outlet of the j-th part of the recuperator. In addition, as reported in (15) and (16), it is important to note that the two aforementioned thermal fluxes are also calculated as a function of global transmittance coefficients ($K_{eg,m}$, $K_{a,m}$), heat exchange surfaces ($S_{eg,m}$, $S_{a,m}$) and logarithmic mean temperature differences ($\Delta T_{lm,eg,m}$, $\Delta T_{lm,a,m}$).

2.5.3. Combustion Chamber

Having already considered the mass accumulations concentrated in block ψ_f, it was decided to model the combustion chamber (CC) as an algebraic block described by steady-state mass and energy balances, in order not to overcomplicate the model and thus reduce the computational effort. The mass balance is shown in (17) and the energy balance in (18).

$$\dot{M}_{a,R} + \dot{M}_f - \dot{M}_{eg} = 0 \quad (17)$$

$$\dot{M}_{a,in,CC} \cdot \bar{c}_{p,a,CC} \cdot (T_{a,in,CC} - T_r) + \dot{M}_f \cdot LHV_f \cdot \eta_{CC} - \dot{M}_{eg} \cdot \bar{c}_{p,eg,CC} \cdot (T_{eg,out,CC} - T_r) = 0 \quad (18)$$

In (17) $\dot{M}_f$ indicates the fuel mass flow rate while, in (18), $\dot{M}_{a,in,CC}$ is the air mass flow rate entering the combustion chamber (equal to $\dot{M}_{a,R}$). $T_{a,in,CC}$ is the air temperature at the inlet of the combustion chamber, assumed to be coincident with $T_{a,out,J}$. T_r is the reference temperature for the evaluation of the fuel lower heating value (LHV_f), $\bar{c}_{p,a,CC}$ and $\bar{c}_{p,eg,CC}$ are average specific heat values for air and exhaust gas, and η_{CC} is the combustion chamber efficiency. The mass balance is used to calculate $\dot{M}_{eg}$, while the exhaust gas temperature at the outlet of the combustion chamber $T_{eg,out,CC}$ is the output of the energy balance.

2.5.4. Turbine

The turbine is assumed to be in chocking conditions. The pressure at the inlet of the turbine ($p_{T,in}$) is then calculated as a function of $\dot{M}_{eg}$ and $T_{eg,out,CC}$, as shown in (19) where the coefficient Γ_T is equal to the ratio $\frac{\dot{M}_{eg} \cdot \sqrt{T_{eg,out,CC}}}{p_{T,in}}$ calculated at nominal steady state (full load).

$$p_{T,in} = \frac{\dot{M}_{eg} \cdot \sqrt{T_{eg,out,CC}}}{\Gamma_T} \quad (19)$$

The turbine outlet temperature $T_{T,out}$ is calculated as:

$$T_{T,out} = T_{T,in} - \eta_T \cdot \left[1 - \frac{1}{\left(\frac{p_{T,in}}{p_{T,out}} \right)^{\frac{k_T - 1}{k_T}}} \right] \quad (20)$$

where the turbine inlet temperature $T_{T,in}$ coincides with $T_{eg,out,CC}$, η_T is the turbine's adiabatic efficiency, $\left(\frac{p_{T,in}}{p_{T,out}} \right)$ the expansion ratio and k_T the adiabatic exponent. Knowing the temperature at the inlet and outlet of the turbine allows to evaluate the real power of the turbine as follows:

$$P_T = \dot{M}_{eg} \cdot \bar{c}_{p,eg,T} \cdot (T_{T,in} - T_{T,out}) \quad (21)$$

where $\bar{c}_{p,eg,T}$ indicates the average specific heat at constant pressure of the exhaust gas. The turbine outlet pressure $p_{T,out}$ is an input to (20) since it is calculated by the algebraic relation (22) which determines it as a function of the external ambient pressure (p_{ext}), the exhaust gas flow rate ($\dot{M}_{eg}$) and the proportionality coefficient δ, similar to the approach adopted in (13).

$$p_{T,out} = \frac{p_{ext}}{\left(1 - \delta \cdot \dot{M}_{eg}^2 \right)} \quad (22)$$

2.5.5. Shaft and Generator

The rotational angular speed ω of the shaft is obtained by integrating (23) which represents the classical dynamic equation for rotating masses. In (23), Y represents the moment of inertia of the MT, η_m the mechanical efficiency, η_G the generator efficiency, and η_{PCS} the efficiency of the power conditioning system that allows the variable speed generator to be coupled to the AC grid at 50 Hz.

$$\frac{d\omega}{dt} = \frac{1}{Y\cdot\omega}\cdot\left[\eta_m\cdot(P_T - P_C) - \frac{P^{el,CHP,des}}{\eta_G\cdot\eta_{PCS}}\right] \tag{23}$$

2.5.6. Heat Recovery Boiler

The heat recovery boiler, which is the heat exchanger used to produce hot water (having a mass flow rate equal to $\dot{M}_w$ and temperature changing from $T_{w,in}$ to $T_{w,out}$) by exploiting the heat released by the exhaust gas at the discharge of the turbine, is modelled using the same approach chosen to model the recuperator in Section 2.5.2.

2.6. CHP Control System

The control system, based on two PIDs, of the MT aims to reset two errors:

- the difference $\varepsilon^{T_{T,out}}$ between the temperature at the turbine outlet ($T_{T,out}$) and its set-point value (that has to be maintained constant according to the specifications provided by the manufacturer);
- the difference ε^{P} between the MT electrical power output $P^{el,CHP}$, calculated as:

$$P^{el,CHP} = \eta_m\cdot\eta_G\cdot\eta_{PCS}\cdot(P_T - P_C) \tag{24}$$

and the desired value $P^{el,CHP,des}$ defined in Equation (6).

Both PIDs generate output signals which are intended to adjust the fuel flow rate in real-time by applying the two quantities $\Delta\dot{M}_f\left(\varepsilon^{T_{T,out}}\right)$ and $\Delta\dot{M}_f\left(\varepsilon^{P}\right)$ that summed up to the quantity $\widetilde{\dot{M}_f}\left(P^{el,CHP,des}\right)$, that represents the fuel necessary to operate the MT at constant load equal to $P^{el,CHP,des}$, give the mass flow rate of fuel $\dot{M}_f$ to be supplied to the combustion chamber:

$$\dot{M}_f = \widetilde{\dot{M}_f}\left(P^{el,CHP,des}\right) + \Delta\dot{M}_f\left(\varepsilon^{T_{T,out}}\right) + \Delta\dot{M}_f\left(\varepsilon^{P}\right) \tag{25}$$

2.7. Thermal Storage System

The dynamic behaviour of the thermal storage system is described by the following differential equation:

$$\frac{dSOC^{STO}}{dt} = \frac{P^{ch,STO} - P^{dch,STO}}{C^{STO,nom}} \tag{26}$$

where SOC^{STO} is the State of Charge, $P^{ch,STO}$ and $P^{dch,STO}$ the charged and discharged thermal power, and $C^{STO,nom}$ the rated thermal capacity; $P^{ch,STO}$ and $P^{dch,STO}$ are defined in accordance with (27) and (28), while thermal losses and degradation effects have been neglected. In particular, $P^{ch,STO}$ is different from zero when the thermal power provided by the MT $P^{th,CHP}$ is greater than the thermal flux $\phi^{PB,req}$ required by the building to guarantee a desired inner temperature. Similarly, $P^{dch,STO}$ is different from zero when $P^{th,CHP}$ is lower than $\phi^{PB,req}$. Upper bounds for $P^{ch,STO}$ and $P^{dch,STO}$ are fixed as well as for SOC^{STO}.

$$P^{ch,STO} = \begin{cases} min\left(P^{ch,STO,max}; P^{th,CHP} - \phi^{PB,req}\right),\ SOC^{STO} < 1 \wedge P^{th,CHP} > \phi^{PB,req} \\ 0,\ P^{th,CHP} \le \phi^{PB,req} \end{cases} \tag{27}$$

$$P^{dch,STO} = \begin{cases} min\left(P^{dch,STO,max}; \phi^{PB,req} - P^{th,CHP}\right),\ SOC^{STO} > 0 \wedge P^{th,CHP} < \phi^{PB,req} \\ 0,\ P^{th,CHP} \ge \phi^{PB,req} \end{cases} \tag{28}$$

https://doi.org/10.3390/en19041064

2.8. Boiler

The boiler, fed by natural gas, acts as a slack. It provides thermal power only if the thermal flux $\phi^{PB,req}$ required by the building is higher than the total power supplied by the MT and the thermal storage system.

$$P^{th,B} = max\left(0;\ \phi^{PB,req} - P^{th,CHP} - P^{dch,STO}\right) \tag{29}$$

2.9. Prosumer Building

Applying the lumped parameter theory, the prosumer building is modelled as a single space characterized by its temperature T^{PB}, which is a function of time. T^{PB} is determined by integrating the energy balance written in dynamic form:

$$\frac{dT^{PB}}{dt} = \frac{1}{C^{PB}} \cdot \left[\phi^{PB,req} - K^{PB} \cdot \left(T^{PB} - T_{ext}\right)\right] \tag{30}$$

where T_{ext} is the outdoor temperature, K^{PB} a global transmittance coefficient and C^{PB} the building's thermal capacity calculated considering the air mass inside the building and the insulation characteristics of the envelope. As shown in (31), the thermal flux $\phi^{PB,req}$ necessary to guarantee a set-point internal temperature ($T^{PB,sp}$) inside the building depends on the error between $T^{PB,sp}$ and T^{PB}, and on the nominal thermal flux $\phi^{PB,req,nom}$ calculated with reference to the design outdoor temperature characterizing the city in which the building is located. A control system made by a PID controller is used to determine $\phi^{PB,req}$.

$$\phi^{PB,req} = \phi^{PB,req}\left(T^{PB}, T^{PB,sp}, \phi^{PB,req,nom}\right) \tag{31}$$

3. Results

The mathematical model presented in Section 2 has been implemented in the Matlab/Simulink R2025a environment. This section shows the main input data of the simulator and describes some simulation results with reference to three different operating conditions, namely a sunny day (Scenario I), a cloudy day (Scenario II) and a rainy day with no PV production (Scenario III). Finally, an additional scenario (Scenario IV) is analyzed, considering a longer simulation time horizon, equal to a winter week, and new input data. Moreover, the calculation of different energy, economic and environmental indicators is reported for the examined scenarios.

3.1. Main Input Data

The considered prosumer building is assumed to be an office building located in the municipality of Savona, in the north of Italy, and owned by a private company operating in the tertiary sector. The choice of this case study is due to the availability of data collected at the Savona Campus of the University of Genoa, where a polygeneration microgrid has been in operation since 2014. The microgrid includes PV plants, CHP units, EV charging points and a battery energy storage system. Regarding CHP units, two CAPSTONE C65 MTs are installed to provide electricity and heating to the buildings of the Campus, which host the facilities of both the university and private companies.

Referring to the different subsystems of the simulator presented in Section 2, the main input data that characterize the case study are described in the following subsections.

3.1.1. Electrical Load

The building is connected to the external Medium-Voltage (MV) 15 kV distribution network with a committed power equal to 250 kW. During the year, the electrical load is around 20 kW in the night hours, while in the central hours of the day, the typical peak values reach 160 kW.

3.1.2. PV Plant Data

The rated peak power of the PV plant is 160 kW. The plant consists of 400 modules (model MaxEON SPR Max3-400 [39]) of 400 W each. The PV modules are installed on the south-oriented roof of the building with a tilt angle of 20°. The PV production has been estimated using the measurements provided by the SCADA system (see [40]) of the Savona Campus microgrid, where three PV plants are currently installed with a total rated power of 120 kW.

3.1.3. EVs and Charging Points

Within the private parking area of the prosumer, four EV charging points are present. Each one is characterized by a maximum AC charging power of 7.4 kW. The four EVs owned by the company are Volkswagen ID.3 Pro [41] model whose main characteristics are reported in Table 1.

Table 1. EV input data.

Rated capacity (C^{EV})	58 kWh
Driving range	405 km
Charging equipment	Type 2 socket for AC charging (11 kW max)
Minimum SOC	0.1
Charging efficiency ($\eta^{ch,EV}$)	0.9

Considering the characteristics of the charging points, the EVs can be charged at a maximum AC power $P^{EV,max}$ of 7.4 kW, when the SOC is in the range between the minimum value and $SOC^{EV,lim}$ assumed equal to 0.8. For higher values of SOC, the maximum power that can be supplied to the EV decreases linearly as a function of SOC.

3.1.4. CHP Unit and Other Thermal Energy Sources

The considered CHP unit is a CAPSTONE C65 microturbine [36]. The main rated data of the CHP unit are reported in Table 2.

Table 2. CHP unit input data.

Rated electrical power	65 kW
Rated thermal power	105 kW
Rated electrical efficiency	0.29
Pressure ratio	4
Minimum electrical power $\left(P^{el,CHP,min}\right)$	30 kW
Exhaust gas mass flow rate at full load	0.49 kg/s
Temperature at the outlet of the combustion chamber at full load	924 °C
Temperature at the outlet of the turbine at full load	638 °C
Temperature of the exhaust gas at the outlet of the recuperator at full load	309 °C

The boiler is characterized by a rated thermal power of 150 kW, while the thermal storage system has a rated capacity $C^{STO,\ nom}$ of 700 kWh.

3.2. Simulation Results—Daily Time Horizon

In the following subsection, the main results of the simulated scenarios are analysed and compared referring to some typical days. The considered time horizon of the simulations is 10 h from 7 A.M. to 5 P.M. of a day in a winter month. For all the scenarios, the electrical load profile, the EV charging demand and the EV availability at the facility stay unchanged.

The four EVs are used by the company staff. The first EV is assumed to arrive at the facility at 8:30 A.M. with a battery SOC of 0.3, and then it leaves at 4:30 P.M. The second EV arrives at 7:30 A.M. with a battery SOC of 0.5 and leaves the facility six hours later. The third EV reaches the facility at 1 P.M. with a battery SOC of 0.3 and remains parked until the end of the simulation. The last EV arrives at 8:30 A.M. with a battery SOC of 0.7 and does not leave the facility for all the remaining simulated time.

As far as the electrical demand profile of the prosumer, it varies between 65 kW and 133 kW during the entire simulation, with higher values from 12 P.M. to 2 P.M.

3.2.1. Simulation Results—Scenario I

The first analyzed scenario considers a sunny day with high PV production. The ambient temperature outside of the building ranges between 2 °C and 8 °C in the morning from 7 A.M. to 10 A.M. and in the afternoon from 4 P.M. to 5 P.M., while in the central hours of the day its values are higher, with a peak around 15 °C at 1 P.M.

In Figure 3, the electrical power profiles of the PV plant (P^{PV}, in yellow), CHP unit ($P^{el,CHP}$, in light green), and EV charging (P^{EV}, in dark green), together with the power injected (P^s, in light blue) and withdrawn (P^b, in red) into/from the distribution network are shown. The PV production profile follows a regular trend that characterizes a typical sunny day, reaching a peak of 110 kW around 12:30 P.M. The CHP unit operating in "electrical priority" works at full load from 7 A.M. to 10 A.M. and from 3:30 P.M. to 5 P.M., while during the central hours of the day its production decreases up to its "technical minimum" of 30 kW. This behavior is due to the high PV production, which almost completely satisfies the electrical demand of the prosumer building. Considering that the CHP unit cannot operate below its "technical minimum" and the large PV production, a surplus of locally produced energy occurs almost at each time instant from 10:30 A.M. to 3 P.M., which is, in turn, injected into the external distribution network. Electricity is mainly withdrawn from the external network in the early morning and after 3 P.M., when the PV production is low. As shown in Figure 3, there are some time intervals in the central hours of the day during which the prosumer building buys electricity since the CHP unit is not able to instantaneously respond to the rapid increase in the electrical demand of the building.

In Figure 4, the thermal power profiles of the CHP unit ($P^{th,CHP}$, in light green), the heat recovery boiler ($P^{th,B}$, in black), the thermal storage discharging ($P^{dch,STO}$, in pink) and charging ($P^{ch,STO}$, in dark green) and the thermal demand of the prosumer building ($\phi^{PB,req}$, in blue) are represented. The thermal demand required by the building follows with some delay the profile of the external ambient temperature over the day. The thermal production of the CHP units stays almost constant before 10 A.M. and after 3:30 P.M., while modulating in the remaining hours due to the strict correlation with electrical production. From 7 A.M. to 9:15 A.M. and between 11 A.M. and 12 P.M., the thermal storage operates in discharging mode when the thermal production of the CHP unit is not sufficient to completely satisfy the thermal demand of the building. From 9:15 A.M. to the end of the considered time horizon, the thermal storage is being charged when the CHP thermal production, even when operating at its "technical minimum", exceeds the required thermal load. The boiler is not used in the presented scenario.

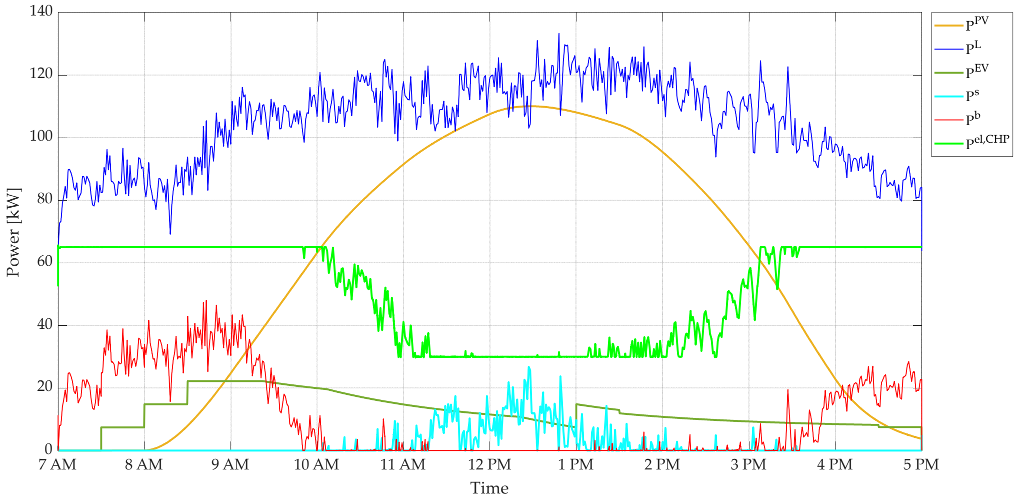

Figure 3. Electrical power profiles for Scenario I.

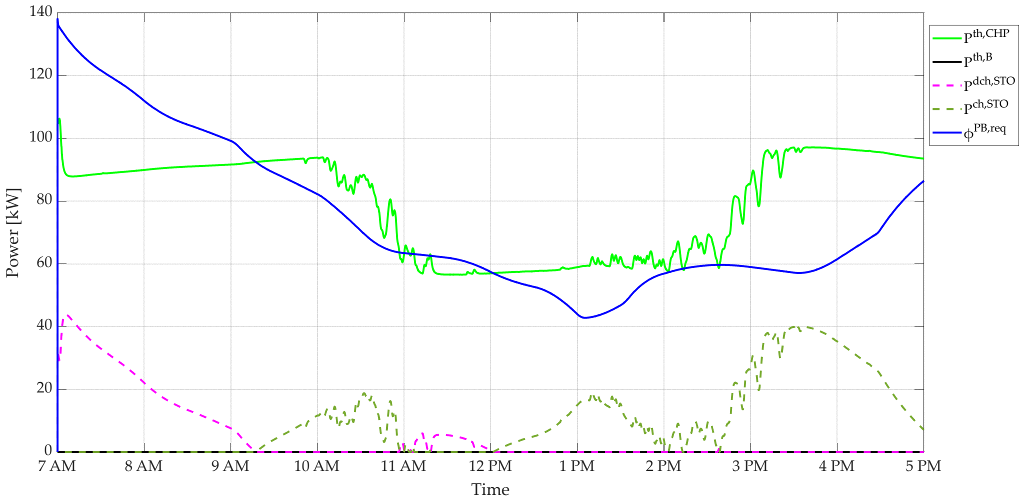

Figure 4. Thermal power profiles for Scenario I.

Figure 5 reports the SOC and charging profiles of the four EVs owned by the prosumer building, which are not enabled to operate in discharging mode. When they are connected to the charging station, the EVs are being charged at their maximum charging power of 7.4 kW until their SOC reaches a value of 0.8.

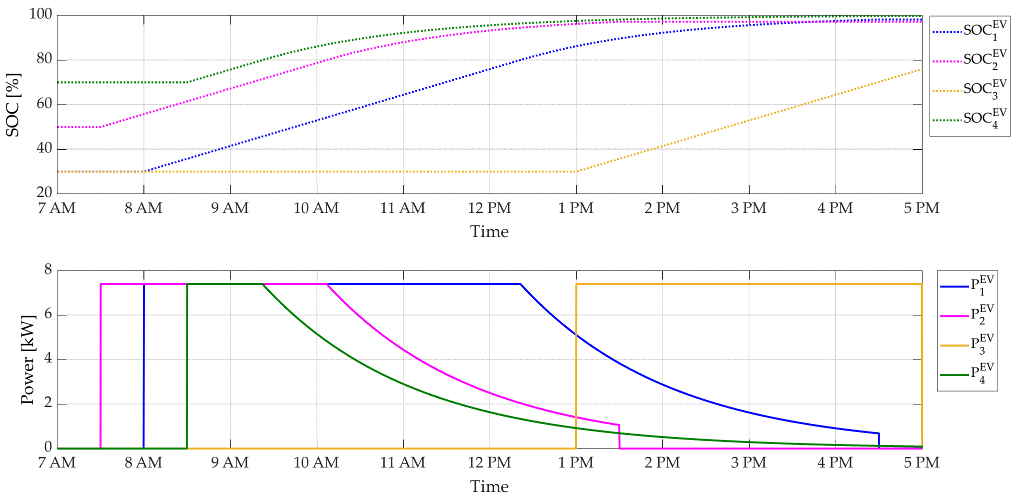

Figure 5. EV charging profiles for Scenario I.

3.2.2. Simulation Results—Scenario II

The second analyzed scenario considers a cloudy day with low PV production while the load profile is kept as in Scenario I. For Scenario II, the ambient temperature outside of the building ranges between 0 °C and 6 °C in the morning from 7 A.M. to 10 A.M. and in the afternoon from 4 P.M. to 5 P.M., while a peak of 10 °C is reached at around 3:30 P.M.

The electrical and thermal power profiles over the considered time horizon are shown in Figures 6 and 7, respectively. In Figure 6, the PV production never reaches 60 kW during the day, and the electrical production of the CHP unit remains constant at its rated power of 65 kW. The power absorbed from the external network is higher when the PV production reaches very low values, e.g., between 12 P.M. and 1 P.M.

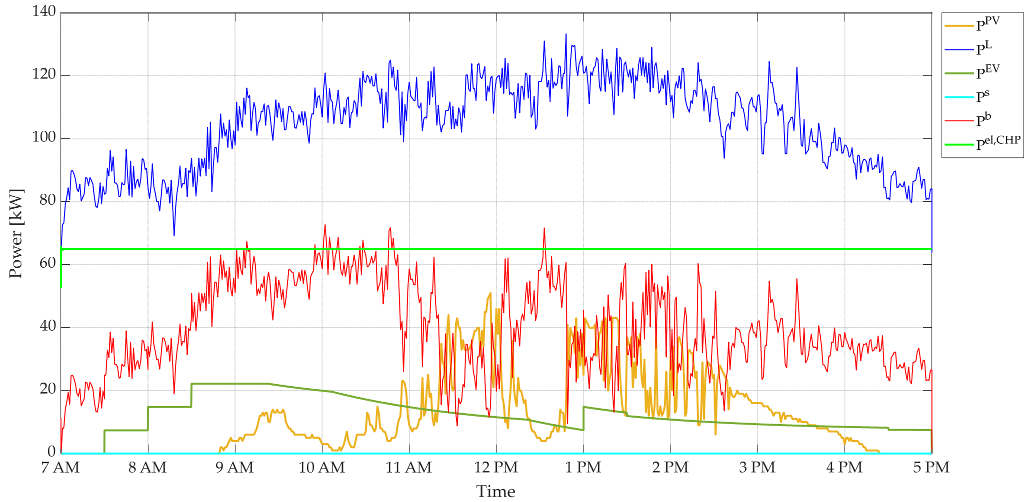

Figure 6. Electrical power profiles for Scenario II.

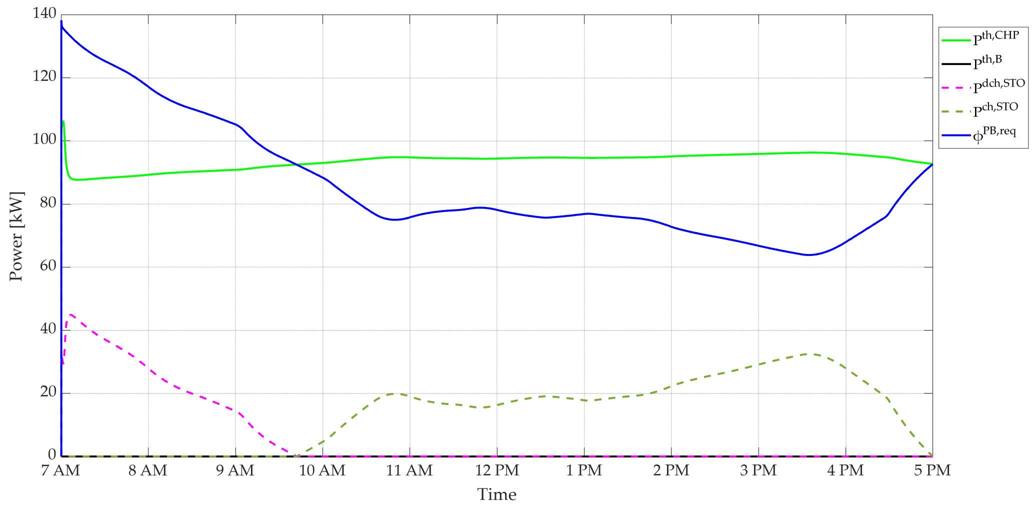

Figure 7. Thermal power profiles for Scenario II.

Concerning thermal power profiles, in Figure 7, the thermal demand of the building follows a trend similar to the one resulting from Scenario I, but with higher average values over the considered time horizon due to the lower external ambient temperature. The CHP thermal production is almost constant, while the thermal storage is discharged from 7 A.M. to 9:45 A.M. and is charged during the remaining hours. Also, for this scenario, the boiler is not in operation.

EV charging profiles are the same as the ones reported in Figure 5.

https://doi.org/10.3390/en19041064

3.2.3. Simulation Results—Scenario III

In the present scenario, representing a rainy day with no PV production during the whole considered time horizon, the ambient temperature outside of the building ranges between −1 °C and 3 °C in the morning from 7 A.M. to 10 A.M., while from 10 A.M. to 5 P.M. its value stays around 6 °C. Figure 8 shows the electrical power profiles: the CHP always operates at its rated power, the building always buys electricity to satisfy its electrical demand and no electricity is sold. The power profile related to the EV charging follows the same trends as the ones reported for Scenario I and Scenario II.

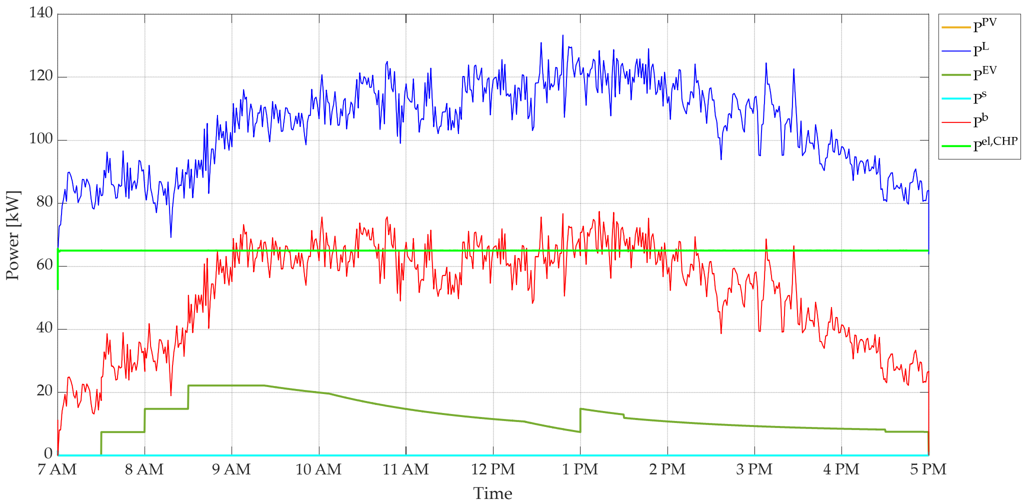

Figure 8. Electrical power profiles for Scenario III.

The thermal power profiles are represented in Figure 9. The thermal demand of the building is always higher than 85 kW, and the CHP unit provides an almost constant thermal power. The thermal storage is discharged from 7 A.M. to 11 A.M. and from 4 P.M. to 5 P.M., while slightly charged from 11 A.M. to 4 P.M.

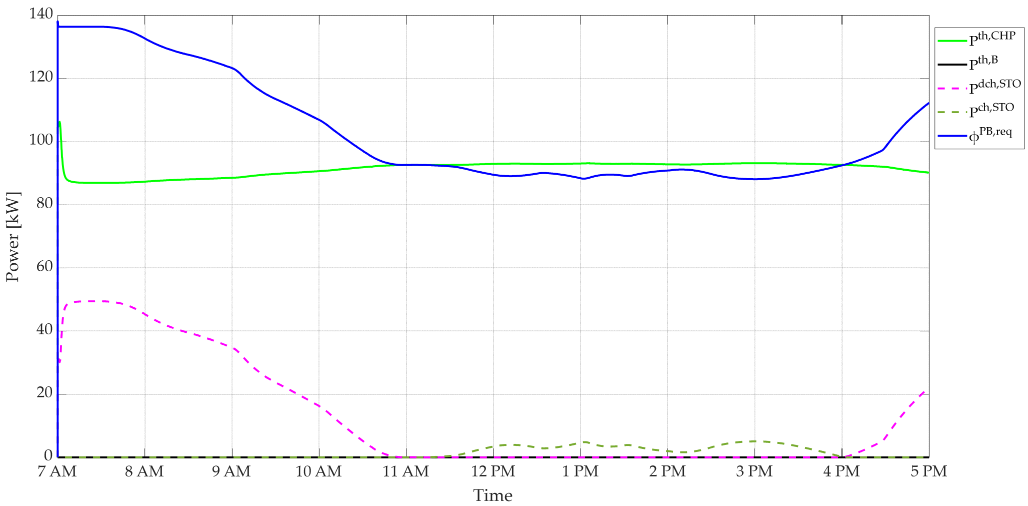

Figure 9. Thermal power profiles for Scenario III.

3.3. Simulation Results—Scenario Comparison

In this subsection, a comparative analysis between the three considered scenarios is carried out, focusing on the main electrical and thermal energy results of the simulation calculated over the whole considered time horizon.

Table 3 reports the electrical energy results, whereas the thermal energy results are shown in Table 4. Compared to Scenario I, Scenario II sees a 79% decrease in total PV production, while CHP electrical production increases by 28.4%; the amount of electricity purchased is 3.8 times larger, and no electricity is sold. In Scenario III, CHP electrical production remains the same as in Scenario II, while electricity purchases increase by 30.4%, due to the absence of PV production. Since the EVs' behavior and the related SOC conditions are not assumed to change in the three different scenarios, the EV charging demand is always equal to 123.1 kWh.

Table 3. Electrical energy results.

kWh	Scenario I	Scenario II	Scenario III
PV production	581.6	121.9	0.0
CHP production	506.1	650.0	650.0
Bought energy	104.9	400.5	522.4
Electrical demand	1049.0	1049.0	1049.0
EV charging demand	123.1	123.1	123.1
Sold energy	20.16	0.0	0.0

Table 4. Thermal energy results.

kWh	Scenario I	Scenario II	Scenario III
CHP production	790.2	935.9	913.9 (913.9)
Boiler production	0.0	0.0	0.0 (126.7)
Thermal storage discharging	51.2	61.3	126.7 (0.0)
Thermal storage charging	101.3	141.6	14.4 (0.0)
Thermal demand	740.1	855.7	1026.0 (1026.0)
Wasted thermal energy	0.0	0.0	0.0 (14.4)

Regarding the thermal part, Table 4 shows a significant increase in the CHP thermal production of 18.4% in Scenario II with respect to Scenario I, since the decrease in the external ambient temperature for Scenario II (i.e., cloudy day) causes a higher thermal demand by the prosumer building (+15.6% compared to Scenario I). This also leads the thermal storage to operate more frequently during the considered time horizon, both in charging and discharging mode, with an increase of 39.8% and 19.7%, respectively, from Scenario I to Scenario II.

Scenario III (i.e., rainy day with no PV production) is characterized by a low thermal storage charged energy since the CHP thermal production, with the contribution of the thermal storage operating in discharging mode, is entirely deployed to satisfy the high thermal demand of the building, due to the very low external ambient temperature during the day.

In all three scenarios, there is no wasted thermal energy, and the boiler is not in operation. To evaluate how the thermal storage operation impacts the thermal energy results of the simulations, an additional analysis related to Scenario III was performed, assuming that the prosumer building is not equipped with thermal storage. The results are reported in parentheses in the column of Scenario III in Table 4. For this additional simulation, the results show that the boiler is required to operate to help the CHP unit satisfy the overall thermal demand of the building (i.e., it supplies the thermal energy

https://doi.org/10.3390/en19041064

previously provided by the thermal storage discharging), and the remaining thermal energy is accounted for as wasted energy since it cannot be stored.

Finally, in order to assess the electrical and thermal operational efficiency of the case study prosumer building, two Key Performance Indicators (KPIs), i.e., the Electrical Self-Sufficiency Rate (ESSR) and the Thermal Storage Utilization Factor (TSUF), can be defined as follows:

$$ESSR = \frac{E^{PV} + E^{el,CHP} - E^{s}}{E^{L} + E^{EV}} \cdot 100 \tag{32}$$

$$TSUF = \frac{E^{dch,STO}}{E^{PB,req}} \cdot 100 \tag{33}$$

where E^{PV}, $E^{el,CHP}$, E^{s}, E^{L}, E^{EV}, $E^{dch,STO}$ and $E^{PB,req}$ are, respectively, the total PV energy production, the CHP electrical energy production, the energy sold to the distribution network, the total electrical load of the building, the total EV charging demand, the total energy discharged by the thermal storage, and the total thermal demand required by the building, calculated over the whole considered time horizon.

The ESSR describes the share of total electrical energy demand of the prosumer building, including the charging of the EVs, covered by the production of the PV and CHP plants. The TSUF is used to quantify the effectiveness of the thermal storage unit in meeting the heating needs of the building over a specific time period.

The results of these KPIs for the three analyzed scenarios are reported in Table 5. As expected, the ESSR has lower values in Scenario II and Scenario III compared to Scenario I, since the PV production significantly decreases in Scenario II (cloudy day) and is equal to zero in Scenario III (rainy day), with the CHP unit satisfying more than half of the total electrical demand of the building (including EV charging needs), both in Scenario II and in Scenario III. On the other hand, the TSUF shows an increase from Scenario I to Scenario II (+4.3%) and to Scenario III (+78.3%) related to the decrease in the ambient temperature outside of the building, which in turn leads to higher thermal demand.

Table 5. KPIs' results for the three scenarios.

[%]	Scenario I	Scenario II	Scenario III
ESSR	91.1	65.9	55.5
TSUF	6.9	7.2	12.3

To better highlight how the proposed dynamic model enhances the prosumer building's performance, additional economic and environmental indicators are defined and calculated. In particular, for all the three scenarios in the *TO-BE* case (characterized by the presence of MT, PV, thermal storage and back-up boiler), the deviations in Net Operating Costs (NOC) and CO_2 emissions are evaluated referring to the *AS-IS* case, where all the electricity needed to satisfy the electrical load of the facility and EV charging demand is exclusively withdrawn from the external distribution network (no PV and no MT installed). All the thermal energy is assumed to be produced by a traditional boiler fed by natural gas. Since the thermal demand of the facility is different in each scenario, due to the different weather conditions, there are three *AS-IS* cases, one for each scenario.

The economic (ΔNOC_s) and environmental (ΔCO_{2s}) percentage deviations for each scenario are calculated as follows:

$$\Delta NOC_s = -\frac{NOC_{s,AS-IS} - NOC_{s,TO-BE}}{NOC_{s,AS-IS}} \cdot 100 \tag{34}$$

$$\Delta CO_{2s} = -\frac{CO_{2s,AS-IS} - CO_{2s,TO-BE}}{CO_{2s,AS-IS}} \cdot 100 \tag{35}$$

where the subscript s indicates the corresponding scenario (Scenario I, Scenario II, or Scenario III).

To assess the total net operating costs of the facility and equivalent CO_2 emissions over the considered time horizon (i.e., 10 h), the following assumptions have been made, taking into account both the type of prosumer and the Italian energy context:

- purchase electricity price equal to 0.25 €/kWh;
- selling electricity price equal to 0.1 €/kWh;
- natural gas price equal to 0.45 €/Sm^3;
- annual maintenance costs of PV plant equal to 20 €/kW_p;
- lower heating value of natural gas equal to 9.59 kWh/Sm^3;
- traditional boiler efficiency equal to 0.9;
- maintenance costs of the MT equal to 2 € per each Equivalent Operating Hour (EOH) of the MT;
- emission factor of the electricity coming from the distribution network equal to 234.7 gCO_2/kWh [42];
- emission factor per unit of primary energy of the traditional boiler (used in the *AS-IS* case) and CHP unit (used in the *TO-BE* case), both fed by natural gas, equal to 205 gCO_2/kWh.

The results of the total net operating costs and CO_2 emissions, and the corresponding percentage deviations with respect to the *AS-IS* cases, are reported for Scenario I (sunny day), Scenario II (cloudy day), and Scenario III (rainy day) in Tables 6 and 7, respectively.

Table 6. Scenario comparison between total net operating costs and CO_2 emissions.

	Total Costs [€]	**[kg CO_2]**
AS-IS		
Scenario I	331.61	443.7
Scenario II	337.64	470.0
Scenario III	346.52	508.8
	Total Costs [€]	**[kg CO_2]**
TO-BE		
Scenario I	133.36	395.2
Scenario II	237.82	569.9
Scenario III	268.30 (274.90)	598.5 (627.4)

Table 7. Economic and environmental deviations for the three scenarios compared to the *AS-IS* case.

[%]	**Scenario I**	**Scenario II**	**Scenario III**
ΔNOC	−59.8	−29.6	−22.6 (−20.7)
ΔCO_2	−10.9	+21.3	+17.6 (+23.3)

Regarding the net operating costs to operate the facility, Scenario I is the best one in the *TO-BE* case, mainly due to the fact that the PV production is significant and the thermal demand is lower than in the other scenarios. In Scenario III, the cost reduction with respect to the *AS-IS* case is the lowest one, especially when the thermal storage is not supposed to be in operation (i.e., −20.7%). Anyway, the installation of MT, PV and thermal storage is profitable for the facility in all three scenarios, as shown by the reduction in total net operating costs reported in Table 6. On the other hand, not all the scenarios in the *TO-BE* case are characterized by lower values of CO_2 emissions compared to the corresponding scenarios in the *AS-IS* case. Indeed, Scenario II and Scenario III show higher CO_2 emissions due to a larger use of MT and back-up boiler, and also an increase in electricity withdrawn from the distribution network because of the lower PV production.

3.4. Simulation Results—Weekly Time Horizon

To better evaluate the building thermal and electrical dynamics and the performance of the installed technologies, a longer simulation time horizon has been analyzed. In this subsection, the main simulation results are presented for a new scenario (Scenario IV), considering a time horizon of a winter week. The weekly PV production has still been estimated through the measurements provided by the SCADA system of the Savona Campus microgrid of the University of Genoa, while the EV charging demand and availability at the building have been changed with respect to the previous scenarios (Scenario I, Scenario II and Scenario III), also considering three additional EVs at the disposal of the prosumer.

In Figure 10, the weekly electrical power profiles are shown. The electrical load follows a similar pattern in the working days with an absorption peak around 150 kW on Wednesday, while it decreases significantly on the weekend up to values around 50 kW. The PV production is consistent from Wednesday to Friday, reaching values around 110 kW, while it is considerably lower on the other days, with values below 20 kW on Sunday. The CHP unit operates at its rated power only on the working days of the week when the electrical load of the building is higher, more EVs need to be charged (such as on Monday and on Tuesday), and there is no PV production (or it is very low) in those hours. The power withdrawn from the distribution network is significant on Monday and on Tuesday to meet the high electrical demand and EV charging needs, and the power production from the PV plant is not sufficient, while it decreases in the following days up to zero on Saturday and on Sunday. On the other hand, the power injected into the external network is very reduced during the whole considered week, with few peaks in the morning from Wednesday to Saturday when there is a surplus of PV production.

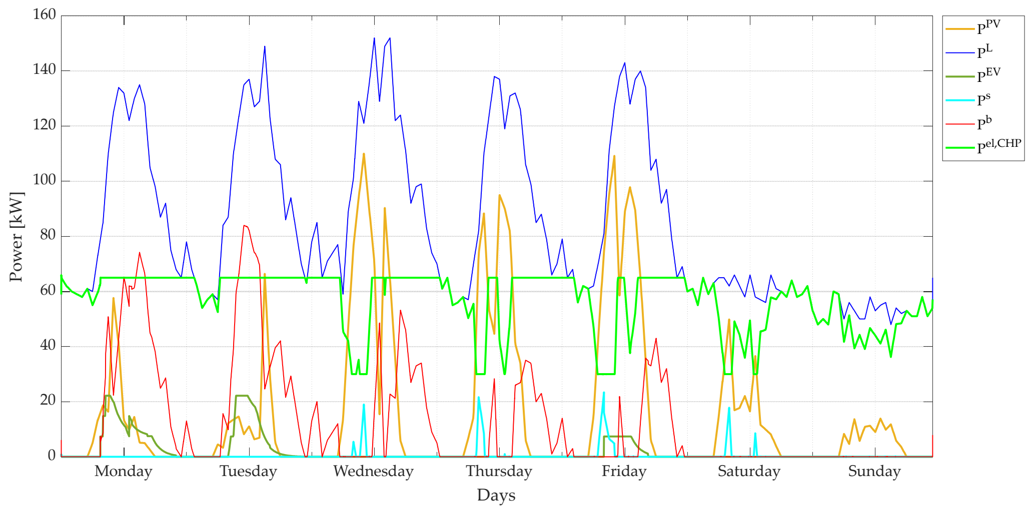

Figure 10. Electrical power profiles for Scenario IV (weekly time horizon).

In Figure 11, the weekly thermal power profiles are shown. The thermal demand of the prosumer building ranges between 40 kW and 105 kW during the week. On Monday and on Tuesday, the thermal power provided by the CHP unit is always higher than the thermal demand and, consequently, the thermal storage is being operated in charging mode. Mainly on Wednesday, on Friday and on Sunday afternoon, the thermal storage is being discharged to help the CHP unit satisfy the thermal load of the building. During the analyzed week, the back-up boiler has never been required to be in operation, and there is no wasted thermal energy. As it can also be noticed from Figure 12, the thermal demand follows the trend of the external ambient temperature (ranging from 3 °C to 14 °C during the week), which reaches lower values, below 5 °C, in the early morning on Wednesday and in the central hours on Friday and higher values, between 11 °C and 14 °C, on Monday and on Saturday morning.

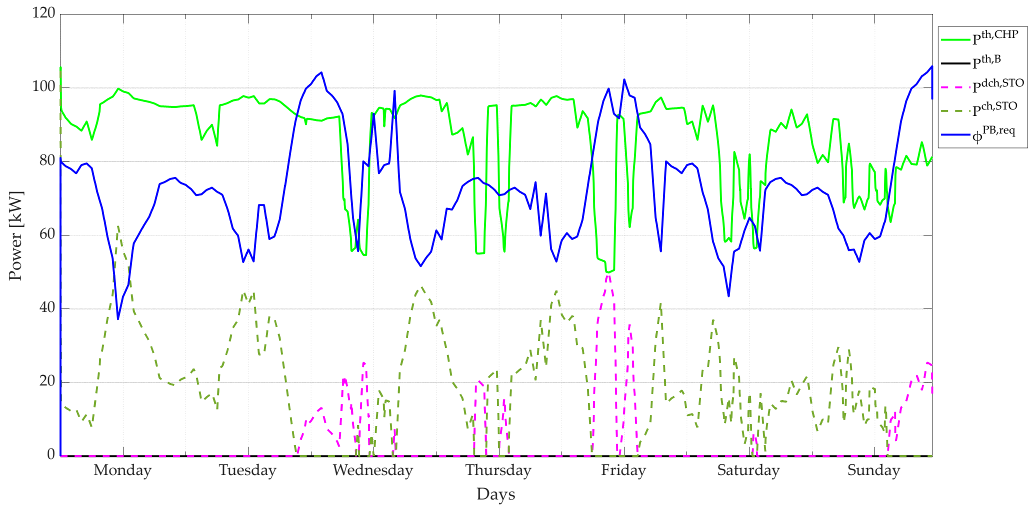

Figure 11. Thermal power profiles for Scenario IV (weekly time horizon).

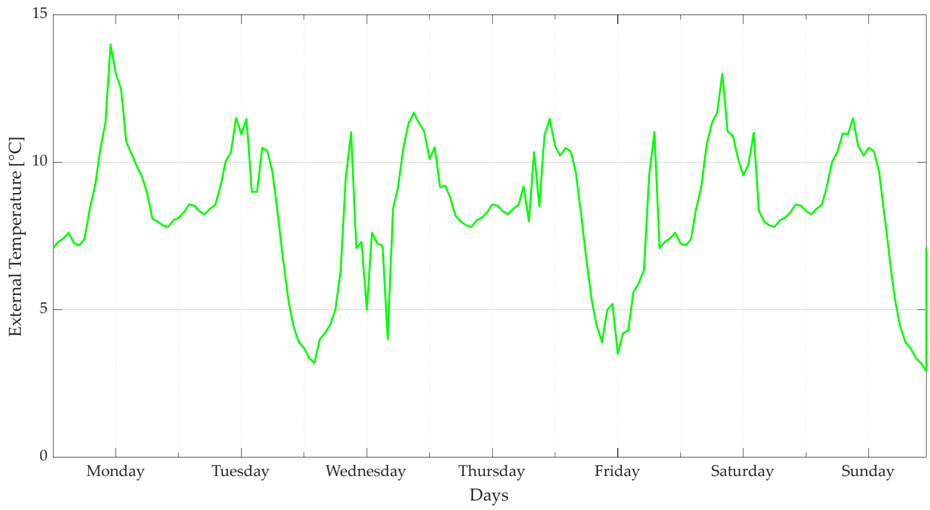

Figure 12. External temperature profile for Scenario IV (weekly time horizon).

Finally, the energy, economic and environmental indicators have also been evaluated for Scenario IV (over a week), as reported in Table 8. The weekly results show a great ESSR due to a large amount of PV and CHP electrical production locally self-consumed, while the thermal storage is not so much exploited in discharging mode since the CHP thermal production largely covers the thermal request of the building, and the back-up boiler is off during the whole week. Concerning the economic and environmental performance, a reduction in total net operating costs of 41.7% occurs with respect to the *AS-IS* case, but CO_2 emissions increase of 21.6%.

Table 8. KPIs' results for Scenario IV (weekly time horizon).

[%]	Scenario IV
ESSR	85.5
TSUF	4.8
ΔNOC	−41.7
ΔCO_2	+21.6

Nowadays, the emission factor of the electricity withdrawn from the distribution network has dropped significantly due to the increasing penetration of RESs in the European network. Consequently, a CHP plant fed by natural gas might lower the overall operational costs but could actually increase the carbon footprint of the facility. To ensure true decarbonization and environmental benefits, the best approach would be to transition toward MTs fueled by biogas or other sustainable fuels.

4. Conclusions

The transformation of existing buildings into multi-energy prosumers represents a pivotal strategy for the decarbonization of urban environments and the strengthening of grid stability. The transition from passive consumers to active multi-energy systems, capable of producing and managing both electrical and thermal power, is essential for a sustainable and resilient energy future.

In this study, a dynamic simulation model of a prosumer building equipped with a PV plant, a CHP unit operated in "electrical priority" mode, a back-up boiler, a thermal storage system and EV charging points has been developed and implemented in the Matlab/Simulink R2025a environment. The aim of the proposed model is to optimize the operation of the installed technologies and to keep a desired comfort inside the building (i.e., to follow a desired temperature profile), by defining different suitable control subsystems within the simulator. The case study building is assumed to be located in the north of Italy and operated by a private company belonging to the tertiary sector, with a 15 kV MV connection to the external distribution network.

The results of the simulation, firstly carried out over a time horizon of 10 h in a winter day (i.e., from 7 A.M. to 5 P.M.), were analyzed for three scenarios according to different values of the external ambient temperature: (i) Scenario I characterized by a sunny day with high PV production and ambient temperature reaching a peak of 15 °C; (ii) Scenario II, where a cloudy day with low PV production and an ambient temperature ranging from 0 °C to 10 °C is considered; and (iii) Scenario III with no PV production (i.e., rainy day) and ambient temperature values not exceeding 6 °C. The energy, economic and environmental performance of the entire system has been evaluated, for each scenario, using four indicators: Electrical Self-Sufficiency Rate (ESSR), Thermal Storage Utilization Factor (TSUF), percentage deviation in total net operating costs (ΔNOC) and in CO_2 emissions (ΔCO_2) with respect to the *AS-IS* case. These demonstrate how a well-designed local electrical and thermal generation system can reduce electricity withdrawal from the distribution network and the use of a backup boiler; indeed, small-sized CHP units coupled with RES plants and storage systems can increase the energy self-sufficiency of prosumer buildings and help to make urban areas smarter. Regarding the net operating costs of the facility and CO_2 emissions, the impact of PV production and CHP operation is significant, highlighting how the profitability and sustainability of a complex multi-energy system are often not correlated and depend on the effective and green operation of the installed technologies. To deepen the analysis and to better assess the electrical and thermal dynamics of the technologies installed at the facility, an additional scenario (Scenario

IV) has been considered over a weekly time horizon, for which the previously defined performance indicators have also been calculated. Also in this longer duration scenario, the installed technologies permit a significant increase in local self-consumption and to reduce net operating costs of the facility, but, on the other hand, CO_2 emissions increase with respect to the *AS-IS* case (+21.6%), due to the fact that the CHP unit is fed by natural gas and not a fuel obtained by RESs exploitation.

The authors intend to expand the simulation model to include other technologies, such as absorption chillers, heat pumps, and battery energy storage systems. Furthermore, they plan to integrate the simulator with a Model Predictive Control Energy Management System to implement the most effective operational strategies for the CHP unit, storage systems, and EV charging points.

Author Contributions: Conceptualization, S.B. and T.R.; methodology, S.B.; software, S.B.; validation, S.B., M.F. and F.S.; data curation, S.B., T.R. and M.F.; writing—original draft preparation, S.B. and T.R.; writing—review and editing, S.M. and F.S.; project administration, S.B., S.M. and F.S.; funding acquisition, S.B., S.M. and F.S. All authors have read and agreed to the published version of the manuscript.

Funding: The publication is part of the project PE0000021, "Network 4 Energy Sustainable Transition—NEST", funded by the European Union—NextGenerationEU, under the National Recovery and Resilience Plan (NRRP), Mission 4 Component 2 Investment 1.3—Concession Decree No. 1561 dated 11 October 2022 of the Ministero dell'Università e della Ricerca (MUR).

Data Availability Statement: Data cannot be disclosed due to confidentiality reasons.

Conflicts of Interest: The authors declare no conflicts of interest.

Abbreviations

The following abbreviations are used in this manuscript:

AC	Alternating Current
C	Compressor
CC	Combustion Chamber
CCHP	Combined Cooling, Heating and Power
CHP	Combined Heat and Power
CS	Control System
DC	Direct Current
DG	Distributed Generation
DR	Demand Response
EL_B	Electrical Balance
EV	Electric Vehicle
L	Load
MT	Micro Turbine
MV	Medium Voltage
PB	Prosumer Building
PV	Photovoltaic
R	Recuperator
RES	Renewable Energy Source
SOC	State Of Charge
STO	Storage
T	Turbine

Nomenclature

The following nomenclature is used in this manuscript:

C	Capacity	Wh
$C_{m,j}$, C^{PB}	Heat capacity	J/K
$\bar{c}_p$	Average specific heat at constant pressure	J/(kg·K)
I^{sol}	Solar irradiance	W/(m^{2}K)
i	Vehicle	-
K	Global transmittance coefficient	W/(m^{2}K)
K^{PB}	Building global transmittance	W/K
k	Adiabatic exponent	-
j	Metal part	-
LHV	Lower Heating Value	J/kg
$\dot{M}$	Mass flow rate	kg/s
$\Delta\dot{M}$	Mass flow rate variation	kg/s
$\widetilde{\dot{M}}_f$	Fuel necessary to operate the microturbine at constant load	
N^{PV}	Number of PV modules	-
n	Rotational speed	rps
P	Power	W
p	Pressure	Pa
S	Heat exchange surface	m^2
SOC	State Of Charge	-
T	Temperature	K
ΔT	Temperature difference	K
t	Time	s
y	Binary indicator	-
α	Azimuth angle	$^\circ$
η	Efficiency	-
δ	Proportionality coefficient	s^2/kg^2
Y	Moment of inertia	kg·m^2
γ	Proportionality coefficient	s^2/kg^2
τ	Tilt angle	$^\circ$
ϕ	Thermal flux	W
ψ_f	Fluid-dynamic capacitance	m·s^2
Γ	Coefficient	s·m·K$^{0.5}$
Λ_f	Fluid-dynamic inductance	m^{-1}
ε	Error	K or W
ω	Rotational angular speed	rad/s

Subscripts

a	Air
C	Compressor
CC	Combustion chamber
eg	Exhaust gas
ext	External
f	Fuel
G	Generator
i	i-th EV
in	Inlet
j	j-th part
lm	Logarithmic mean
m	Metal (or mechanical)
out	Outlet
PCS	Power Conditioning System

R	Recuperator
r	Reference
T	Turbine

Superscripts

arr	Arrival
B	Boiler
b	Bought
CHP	Combined Heat and Power
ch	Charging
dch	Discharging
des	Desired
EV	Electric Vehicle
el	Electrical
L	Load
lim	Limit
max	Maximum
min	Minimum
nom	Nominal
P	Power
PB	Prosumer Building
PV	Photovoltaic
req	Required
s	Sold
sol	Solar
sp	Set-point
STO	Storage
T_T	Turbine temperature
th	Thermal

References

1. Nadalipour Kaldeh, S.; Yousefi, H.; Noorollahi, Y.; Abdoos, M. Integration of Renewable Sources in Buildings: A Review of Energy Savings, Feasibility, and Challenges. *Energy Rep.* **2025**, *14*, 3905–3934. [CrossRef]
2. Canelli, M.; Entchev, E.; Sasso, M.; Yang, L.; Ghorab, M. Dynamic Simulations of Hybrid Energy Systems in Load Sharing Application. *Appl. Therm. Eng.* **2015**, *78*, 315–325. [CrossRef]
3. Ghanem, R.S.; Nousch, L.; Richter, M. Modeling of a Grid-Independent Set-Up of a PV/SOFC Micro-CHP System Combined with a Seasonal Energy Storage for Residential Applications. *Energies* **2022**, *15*, 1388. [CrossRef]
4. Annuk, A.; Yaïci, W.; Lehtonen, M.; Ilves, R.; Kabanen, T.; Miidla, P. Simulation of Energy Exchange between Single Prosumer Residential Building and Utility Grid. *Energies* **2021**, *14*, 1553. [CrossRef]
5. Guda, S.R.; Wang, C.; Nehrir, M.H. A Simulink-Based Microturbine Model for Distributed Generation Studies. In *Proceedings of the 37th Annual North American Power Symposium*; IEEE: Ames, IA, USA, 2005; pp. 269–274.
6. Wang, Y.; Bermukhambetova, A.; Wang, J.; Lv, J.; Gao, Q. Dynamic Modelling and Simulation Study of a University Campus CHP Power Plant. In *Proceedings of the 2014 20th International Conference on Automation and Computing*; IEEE: Cranfield, UK, 2014; pp. 3–8.
7. Dutra, J.C.; Gonzalez Carmona, M.A.; Lazaro Alvarado, A.F.; Coronas, A. Modeling of a Cogeneration System with a Micro Gas Turbine Operating at Partial Load Conditions. *J. Sustain. Dev. Energy Water Environ. Syst.* **2017**, *5*, 139–150. [CrossRef]
8. Koch, K.; Höfner, P.; Gaderer, M. Techno-Economic System Comparison of a Wood Gas and a Natural Gas CHP Plant in Flexible District Heating with a Dynamic Simulation Model. *Energy* **2020**, *202*, 117710. [CrossRef]
9. Sartor, K.; Quoilin, S.; Dewallef, P. Simulation and Optimization of a CHP Biomass Plant and District Heating Network. *Appl. Energy* **2014**, *130*, 474–483. [CrossRef]
10. Glavan, I.; Prelec, Z.; Pavkovic, B. Modelling, Simulation and Optimization of Small-Scale CCHP Energy Systems. *Int. J. Simul. Model.* **2015**, *14*, 683–696. [CrossRef]
11. Cao, Y.; Hu, H.; Chen, R.; Si, F. Operation Optimization for a CHP System Using an Integrated Approach of ANN and Simulation Database. *Appl. Therm. Eng.* **2025**, *266*, 125771. [CrossRef]

12. Das, B.K.; Al-Abdeli, Y.M. Optimisation of Stand-Alone Hybrid CHP Systems Meeting Electric and Heating Loads. *Energy Convers. Manag.* **2017**, *153*, 391–408. [CrossRef]
13. Smaisim, G.F.; Abed, A.M.; Hadrawi, S.K.; Majdi, H.S.; Shamel, A. Modelling and Optimization of Combined Heat and Power System in Microgrid Based on Renewable Energy. *Clean Energy* **2023**, *7*, 735–746. [CrossRef]
14. Huang, P.; Lovati, M.; Zhang, X.; Bales, C.; Hallbeck, S.; Becker, A.; Bergqvist, H.; Hedberg, J.; Maturi, L. Transforming a Residential Building Cluster into Electricity Prosumers in Sweden: Optimal Design of a Coupled PV-Heat Pump-Thermal Storage-Electric Vehicle System. *Appl. Energy* **2019**, *255*, 113864. [CrossRef]
15. Liu, Z.; Chen, Y.; Zhuo, R.; Jia, H. Energy Storage Capacity Optimization for Autonomy Microgrid Considering CHP and EV Scheduling. *Appl. Energy* **2018**, *210*, 1113–1125. [CrossRef]
16. Ragab, M.M.; Ibrahim, R.A.; Desouki, H.; Swief, R. A Probabilistic Renewable Energy Allocation Applying Metaheuristics Optimization Methodologies. In *Proceedings of the 2023 11th International Conference on Smart Grid (icSmartGrid)*; IEEE: Paris, France, 2023; pp. 1–6.
17. Ragab, M.M.; Ibrahim, R.A.; Desouki, H.; Swief, R. Optimal Energy Management Applying Load Elasticity Integrating Renewable Resources. *Sci. Rep.* **2023**, *13*, 15000. [CrossRef]
18. Elkadeem, M.R.; Abido, M.A. Optimal Planning and Operation of Grid-Connected PV/CHP/Battery Energy System Considering Demand Response and Electric Vehicles for a Multi-Residential Complex Building. *J. Energy Storage* **2023**, *72*, 108198. [CrossRef]
19. Ma, L.; Liu, N.; Zhang, J.; Tushar, W.; Yuen, C. Energy Management for Joint Operation of CHP and PV Prosumers Inside a Grid-Connected Microgrid: A Game Theoretic Approach. *IEEE Trans. Ind. Inf.* **2016**, *12*, 1930–1942. [CrossRef]
20. Suárez, I.; Prieto, M.M.; Fernández, F.J. Analysis of Potential Energy, Economic and Environmental Savings in Residential Buildings: Solar Collectors Combined with Microturbines. *Appl. Energy* **2013**, *104*, 128–136. [CrossRef]
21. Aguiar, A.B.M.; Pinto, J.O.P.; Andrea, C.Q.; Nogueira, L.A.H. Modeling and Simulation of Natural Gas Microturbine Application for Residential Complex Aiming Technical and Economical Viability Analysis. In *Proceedings of the 2007 IEEE Canada Electrical Power Conference*; IEEE: Montreal, QC, Canada, 2007; pp. 376–381.
22. Pirkandi, J.; Jokar, M.A.; Sameti, M.; Kasaeian, A.; Kasaeian, F. Simulation and Multi-Objective Optimization of a Combined Heat and Power (CHP) System Integrated with Low-Energy Buildings. *J. Build. Eng.* **2016**, *5*, 13–23. [CrossRef]
23. Grillo, S.; Massucco, S.; Morini, A.; Pitto, A.; Silvestro, F. Microturbine Control Modeling to Investigate the Effects of Distributed Generation in Electric Energy Networks. *IEEE Syst. J.* **2010**, *4*, 303–312. [CrossRef]
24. Kim, I.; James, J.-A.; Crittenden, J. The Impact of Microturbines and PV Systems of Office Buildings in Energy-Efficient, Economical, and Environmental Aspects. In *Proceedings of the 2015 North American Power Symposium (NAPS)*; IEEE: Charlotte, NC, USA, 2015; pp. 1–6.
25. Khan, S.; Sudhakar, K.; Bin Yusof, M.H. Building Integrated Photovoltaics Powered Electric Vehicle Charging with Energy Storage for Residential Building: Design, Simulation, and Assessment. *J. Energy Storage* **2023**, *63*, 107050. [CrossRef]
26. Buonomano, A.; Calise, F.; Cappiello, F.L.; Palombo, A.; Vicidomini, M. Dynamic Analysis of the Integration of Electric Vehicles in Efficient Buildings Fed by Renewables. *Appl. Energy* **2019**, *245*, 31–50. [CrossRef]
27. Uchman, W. The Cost of Increasing Prosumer Self-Sufficiency. *Appl. Therm. Eng.* **2021**, *186*, 116361. [CrossRef]
28. Kallio, S.; Siroux, M. Exergy and Exergo-Economic Analysis of a Hybrid Renewable Energy System under Different Climate Conditions. *Renew. Energy* **2022**, *194*, 396–414. [CrossRef]
29. Uchman, W.; Kotowicz, J.; Li, K.F. Evaluation of a Micro-Cogeneration Unit with Integrated Electrical Energy Storage for Residential Application. *Appl. Energy* **2021**, *282*, 116196. [CrossRef]
30. Baumann, L.; Boggasch, E. Experimental Assessment of Hydrogen Systems and Vanadium-Redox-Flow-Batteries for Increasing the Self-Consumption of Photovoltaic Energy in Buildings. *Int. J. Hydrogen Energy* **2016**, *41*, 740–751. [CrossRef]
31. Bottecchia, L.; Lubello, P.; Zambelli, P.; Carcasci, C.; Kranzl, L. The Potential of Simulating Energy Systems: The Multi Energy Systems Simulator Model. *Energies* **2021**, *14*, 5724. [CrossRef]
32. Zhang, S.; Hu, X.; He, X.; Tang, S.; Li, H.; Zhang, D. Dynamic Coupling across Energy Forms and Hybrid Simulation of the Multi-Energy System. *Front. Energy Res.* **2023**, *11*, 1209845. [CrossRef]
33. Abbà, I.; La Bella, A.; Corgnati, S.P.; Corsetti, E. Assessing Flexibility in Networked Multi-Energy Systems: A Modelling and Simulation-Based Approach. *Energy Rep.* **2024**, *11*, 384–393. [CrossRef]
34. Keiner, D.; Ram, M.; Barbosa, L.D.S.N.S.; Bogdanov, D.; Breyer, C. Cost Optimal Self-Consumption of PV Prosumers with Stationary Batteries, Heat Pumps, Thermal Energy Storage and Electric Vehicles across the World up to 2050. *Sol. Energy* **2019**, *185*, 406–423. [CrossRef]
35. Liu, R.; Liu, Z.; Leng, Y.; Li, B.; Wu, Y. Economic Model Predictive Control for an Office Building with Photovoltaic, Heat Pump, Thermal Storage and Electric Vehicle under Time-of-Use Tariff. *Build. Environ.* **2025**, *282*, 113312. [CrossRef]
36. Bracco, S.; Delfino, F. A Mathematical Model for the Dynamic Simulation of Low Size Cogeneration Gas Turbines within Smart Microgrids. *Energy* **2017**, *119*, 710–723. [CrossRef]
37. MathWorks MATLAB. Available online: https://it.mathworks.com/products/matlab.html (accessed on 1 February 2026).

38. Laurini, B.; Bonvini, B.; Bracco, S. Optimal Design Model for a Public-Private Renewable Energy Community in a Small Italian Municipality. *Sustain. Energy Grids Netw.* **2024**, *40*, 101545. [CrossRef]
39. SunPower Global Pannelli Fotovoltaici SunPower Maxeon. Available online: https://www.sunpowerglobal.com/it/privati/prodotti/pannelli-fotovoltaici-sunpower-maxeon (accessed on 24 November 2025).
40. Delfino, F.; Procopio, R.; Rossi, M.; Bracco, S.; Brignone, M.; Robba, M. *Microgrid Design and Operation: Toward Smart Energy in Cities*; Artech House power engineering series; Artech House: Boston, MA, USA; London, UK; Norwood, MA, USA, 2018; ISBN 978-1-63081-151-8.
41. EV Database Volkswagen ID.3 Pro (2023–2024) Price and Specifications. Available online: https://ev-database.org/car/1831/Volkswagen-ID3-Pro (accessed on 27 November 2025).
42. Istituto Superiore per la Protezione e la Ricerca Ambientale (ISPRA) Le Emissioni Di CO_2 Nel Settore Elettrico Nazionale e Regionale. Available online: https://emissioni.sina.isprambiente.it/wp-content/uploads/2025/05/Le-emissioni-di-CO2-nel-settore-elettrico_r413-2025_def.pdf (accessed on 28 January 2026).